A facile route to realize ultraviolet emission in a nano-engineered SnO_2-based light-emitting diode

2015 J. Phys. D: Appl. Phys. 48 465103

(http://iopscience.iop.org/0022-3727/48/46/465103)

IOP Publishing Journal of Physics D: Applied Physics
J. Phys. D: Appl. Phys. **48** (2015) 465103 (7pp) doi:10.1088/0022-3727/48/46/465103

A facile route to realize ultraviolet emission in a nano-engineered SnO_2-based light-emitting diode

Yanan Huang[1], Yongfeng Li[1,2], Bin Yao[1,2], Zhanhui Ding[1], Rui Deng[3], Ligong Zhang[4] and Haifeng Zhao[4]

[1] State Key Laboratory of Superhard Materials, College of Physics, Jilin University, Changchun 130012, People's Republic of China
[2] Key Laboratory of Physics and Technology for Advanced Batteries (Ministry of Education), College of Physics, Jilin University, Changchun 130012, People's Republic of China
[3] School of Materials Science and Engineering, Changchun University of Science and Technology, Changchun 130022, People's Republic of China
[4] Key Laboratory of Excited State Processes, Changchun Institute of Optics, Fine Mechanics and Physics, Chinese Academy of Sciences, Changchun 130033, People's Republic of China

E-mail: liyongfeng@jlu.edu.cn and binyao@jlu.edu.cn

Received 23 May 2015, revised 16 September 2015
Accepted for publication 18 September 2015
Published 20 October 2015

Abstract

We reported a facile route to fabricate a tin dioxide (SnO_2)-based light-emitting diode (LED) and obtain an electrically pumped band-edge ultraviolet (UV) emission. We first investigated the photoluminescence (PL) properties of the SnO_2 thin films deposited on quartz substrates annealed at various temperatures. It was found that SnO_2 nanocrystals were embedded in the SnO_2 amorphous matrix after annealing at 400 °C to form a SnO_2 nanoparticle/amorphous hybrid film; the band-edge UV emission was observed from the hybrid film due to the hybrid structure breaking the dipole-forbidden rule of bulk SnO_2. This hybrid SnO_2 film was then deposited on a p-type GaN substrate to form a SnO_2 hybrid film-based LED and a band-edge UV electroluminescence (EL) was observed. Our results suggest that this easy and effective approach may find extensive application in the field of optoelectronics, displays and solid-state lighting.

Keywords: tin dioxide, dipole-forbidden rule, photoluminescence, electroluminescence, light-emitting diode

(Some figures may appear in colour only in the online journal)

1. Introduction

The exploitation of wide-bandgap transparent oxide semiconductors has drawn much attention for quite some time due to their excellent optical and electrical properties [1–5]. Tin dioxide (SnO_2), as one of these wide-bandgap materials, is widely used in applications such as transparent conducting thin films, gas sensors, solar cells, light-emitting diodes (LEDs) and so on [6–12]. SnO_2 is an n-type semiconductor with a wide direct bandgap of ~3.6 eV and a large exciton-binding energy of ~130 meV. However, many reports showed a superior broad photoluminescence (PL) band in the visible range; no ultraviolet (UV) PL peak was observed as a result of the dipole-forbidden nature of band-edge quantum states for bulk SnO_2 [13], which has imposed restrictions on the application of SnO_2 in the UV optoelectronic field, especially in relation to UV LEDs and photodiodes. The properties of bulk SnO_2 are obviously different from other oxides, such as zinc oxide (ZnO) which has strong near-band-edge emissions and can be applied to the field of UV light emission [14–23]. Nevertheless, with the arrival of nanotechnology, a lot of researchers began to study the nanostructures of SnO_2, such as nanowires, nanorods and quantum dots [9, 24–30]. Eventually, UV emission in the nanostructure of SnO_2 was observed as a result of breaking

the dipole-forbidden rule. In our previous work, to break the dipole-forbidden rule and realize near-band-edge UV emission from SnO_2, the tailored low-temperature annealing process was used to obtain SnO_2 nanocrystals in an amorphous matrix structure and indium was doped into the SnO_2 to modify the band-edge symmetry. Using these methods, UV LEDs were fabricated and UV electroluminescence (EL) was observed [6, 9]. However, there exists disadvantage with these methods. For example, the magnesium oxide (MgO) dielectric layer has to be inserted between the SnO_2 and gallium nitride (GaN) layer as an electron-blocking layer to obtain dominant UV emission, which makes the fabrication process complicated. Therefore, it is necessary to develop an easier effective method of realizing dominant UV emission, such as via a SnO_2-based LED without a MgO layer.

In this paper, an UV emission was observed from a SnO_2 nanocrystal/amorphous hybrid thin film. Such a hybrid thin film was deposited on a p-GaN substrate to form a SnO_2-based LED, in which an electrically pumped UV dominant emission was also observed. The fabrication process of a LED is very easy, which makes SnO_2 nanomaterial more easily applied to the UV optoelectronic field.

2. Experimental process

SnO_2 thin films with a thickness of 1600 nm were deposited on quartz substrates at room temperature using pure argon (Ar) as the working gas by using the radio frequency (rf) magnetron sputtering method. A commercially available high-purity SnO_2 target (purity $> 99.99\%$) with stoichiometric proportion was used in our experiments. The vacuum chamber was evacuated to a base pressure of 10^{-4} Pa before deposition and the sputtering pressure for SnO_2 was controlled to 0.1 Pa. The sputtering power was 100 W. The Ar flow rate was kept at 30 SCCM. In order to wipe off impurities on the surface of the SnO_2 target, the target was pre-sputtered by Ar gas for 10 min before the SnO_2 layer was deposited on the substrate. The growth time of the SnO_2 was one hour. The SnO_2/quartz samples were annealed at 400, 600 and 800 °C in air for 30 min in a horizontal quartz tube furnace, respectively. When the temperature of the tube furnace reached annealing temperature, the SnO_2/quartz samples were put into it. After annealing for 30 min, the samples were taken out and cooled to room temperature. For the preparation of the SnO_2-based heterojunction LED, the SnO_2 layer was deposited on a p-type GaN substrate, to obtain a SnO_2/p-GaN heterojunction, which was annealed at 400 °C in air. The nickel/gold (Ni/Au) electrodes were deposited through a shadow mask on the p-type GaN layer by using a vacuum evaporation method and served as the p-type electrode. Indium metal was used as the n-type contact to the SnO_2 layer. It was pasted on the surface of the SnO_2 film, and then heated on a hot plate; the temperature was fixed at 280 °C and lasted for 3 min, and all this operated in a glove box in order to avoid the oxidation of the sample.

The crystal structure characterization was performed by using x-ray diffraction (XRD) with Cu K_α radiation of 0.154 06 nm. The composition of the thin films was determined using an energy dispersive spectrum (EDS) analyzer. The optical absorption measurements were performed using an UV-vis-near-IR spectrophotometer. The PL measurement was performed using a He-Cd laser with a 325 nm line as the excitation source. A high-resolution transmission electron microscope (TEM) and field emission scanning electron microscopy (FESEM) were used to examine the crystalline structure. The electrical transport parameters of the films were obtained from measuring the resistivity and the Hall coefficient, carried out at room temperature using the van der Pauw method. The current–voltage curves were measured at room temperature to further verify the formation of the p-n heterojunction. The EL measurements were performed using a spectrometer and the current power source as an excite source.

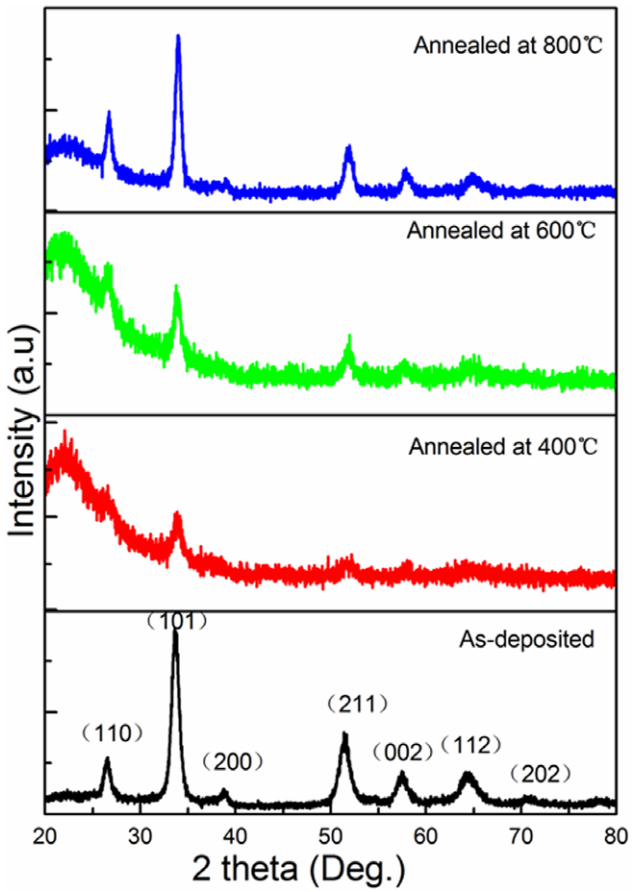

Figure 1. X-ray diffraction patterns of the as-deposited, 400, 600 and 800 °C annealed SnO_2 thin films grown on quartz substrates. All diffraction peaks in these samples are attributed to the SnO_2 films and no other phases are observed.

3. Results and discussion

Figure 1 shows the typical XRD patterns of the as-deposited 400, 600 and 800 °C annealed SnO_2 films deposited on the quartz substrates. The matching of the observed 2θ values in all films with those of standard SnO_2 peaks (PDF#721147) confirms that these thin films are of single-phase with a tetragonal rutile structure. For the as-deposited SnO_2 film, the intensity of all the crystallographic planes' diffraction peaks is very

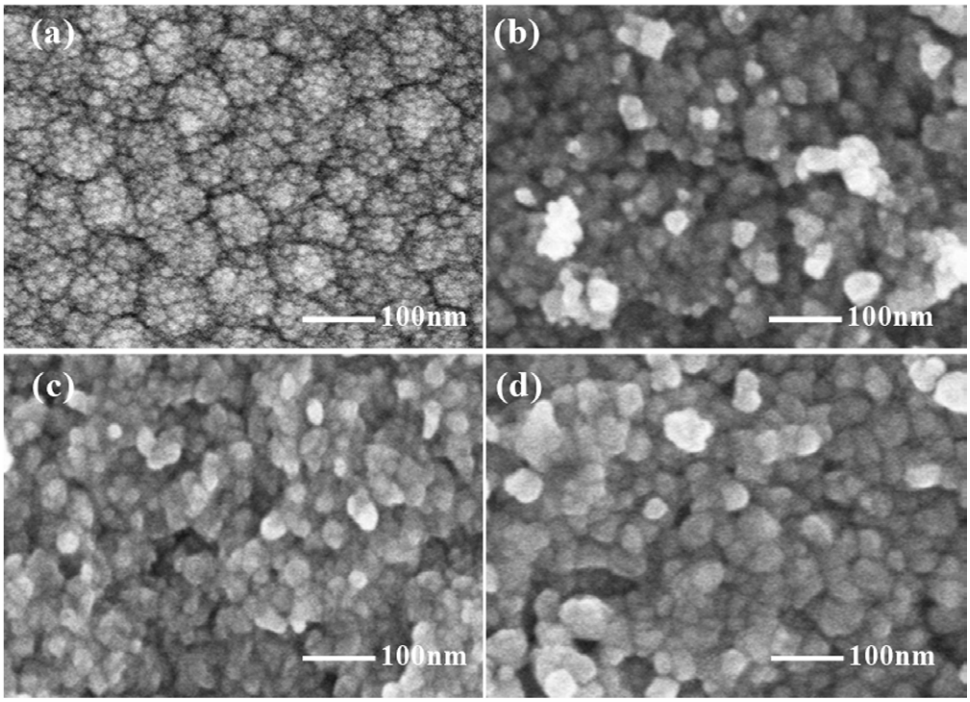

Figure 2. FESEM images of the (a) as-deposited, (b) 400 °C, (c) 600 °C and (d) 800 °C annealed SnO_2 films. The as-deposited film shows an agglomerated structure. After being annealed, particles are formed and then disperse.

strong, which illustrates that the crystallinity is very good. However, the intensity of the diffraction peaks weakens after being annealed at 400 °C, suggesting that the crystallinity of those films declines after they have been annealed. With an increase in the annealing temperature, the intensity of all the crystallographic planes' diffraction peaks enhances, indicating that the crystallinity of the films becomes better once again. Crystalline grain sizes are estimated from XRD data using Scherrer's theorem: $D = k\lambda/\beta\cos\theta$, where k is the shape factor ($k = 0.9$), λ is the x-ray wavelength ($\lambda = 0.15406$ nm) and β is the line broadening in radians at half the maximum intensity. The estimations indicate that the grain sizes are 11.53, 9.07, 10.33 and 10.65 nm for the as-deposited film and the annealed films, respectively. However, it should be noted that it may be incorrect to estimate the grain size using Scherrer's theorem as the film is fully crystallized; many factors (not only grain size) lead to the broadening of the diffraction peak, such as residual stress. Furthermore, the interplanar spacing d of the (hkl) planes in a tetragonal unit cell is given in terms of the lattice constants a and c, by the relation: $1/d^2 = ((h^2 + k^2)/a^2) + l^2/c^2$, where h, k and l are the Miller indices of the diffracting planes. The lattice constants a and c calculated from the d-spacing corresponding to the (1 0 1) and (2 1 1) sets of planes are 5.24 and 3.56, 5.20 and 3.55, 5.21 and 3.55, 5.21 and 3.52 Å for the as-deposited film and annealed films, respectively. It is noted that the calculated values of the lattice parameters for the as-deposited SnO_2 film are larger than the annealed SnO_2 films.

Figure 2 shows the FESEM images of the as-deposited, 400, 600 and 800 °C annealed SnO_2 films grown on quartz substrates. The as-deposited film shows an agglomerated structure. After being annealed, the particles are formed and then disperse. To further investigate the crystalline structure and the evolution of the grain size, TEM and Raman spectroscopy measurements were performed. Figure 3 shows the high-resolution TEM images of the as-deposited and the 400 °C annealed SnO_2 films. It is clearly observed that the as-deposited SnO_2 film is polycrystalline in structure, and that the crystalline grains combine with each other very closely. For the 400 °C annealed SnO_2 film, the nanocrystals are surrounded by the amorphous matrix, forming a nanocrystalline/amorphous hybrid structure. Raman spectra of all samples are shown in figure 4. The mode A_{1g} peaks are found at 633.6, 622.9, 626.3 and 631.9 cm^{-1} for the as-deposited and the 400, 600 and 800 °C annealed SnO_2 films, respectively. The A_{1g} mode is sensitive to the grain size and shifts to lower wave numbers with the decreasing grain sizes [31–33]. Their intensities are reduced then enhanced with the increasing annealing temperature, indicating the process of the crystal-to-amorphous-to-crystal transition. Another kind of peak located at about 500 cm^{-1} is observed, which is attributed to the impurity in the quartz substrate [34]. This result is in good agreement with the changes in the XRD patterns and the TEM images, so the crystallinity of the SnO_2 film after being annealed at 400 °C goes down, forming a nanocrystalline/amorphous hybrid structure. This is the first time a crystal-to-amorphous transition for a SnO_2 film has been seen, but this phenomenon has been studied for other compounds [35, 36]. In contrast to findings from our previous work, the SnO_2 films deposited at room temperature by pulsed laser deposition and sol-gel methods are amorphous, and the crystallinity of those films becomes better after being annealed. In the present work, the SnO_2 film made by rf magnetron sputtering is crystallographic, and the SnO_2 grains contact to each other closely. Although we did not carry out detailed studies on the causes of the crystal-to-amorphous transition and it undoubtedly merits further investigation, we speculated that the

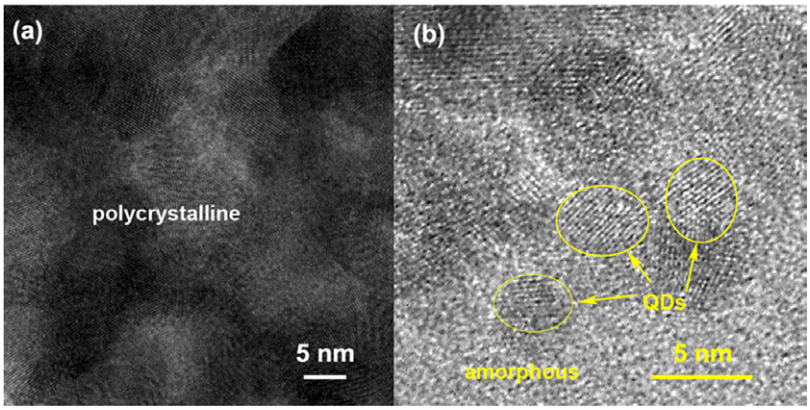

Figure 3. High resolution TEM images of the (a) as-deposited and (b) 400 °C annealed SnO_2 films. The as-deposited SnO_2 film is polycrystalline in structure and the crystalline grains combine with each other very closely. For the 400 °C annealed SnO_2 film, nanocrystals are surrounded by the amorphous matrix, forming a nanocrystalline/amorphous hybrid structure.

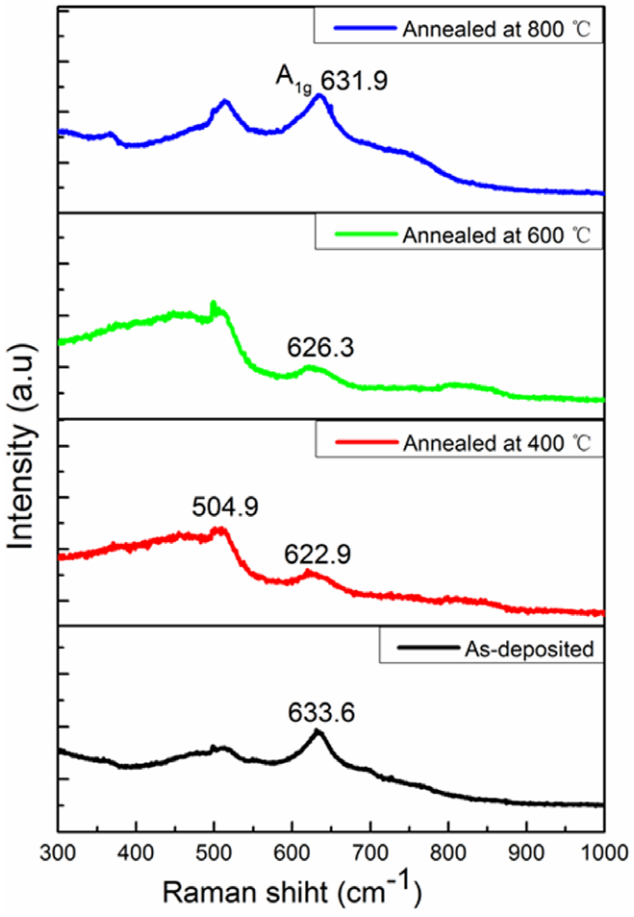

Figure 4. Raman spectra of the as-deposited, 400 °C, 600 °C and 800 °C annealed SnO_2 films.

Table 1. The stoichiometric ratio of Sn and O elements in all the films.

	As-deposited	Annealed at 400 °C	Annealed at 600 °C	Annealed at 800 °C
Sn	34.76%	34.47%	34.82%	34.49%
O	65.24%	65.53%	65.18%	65.51%

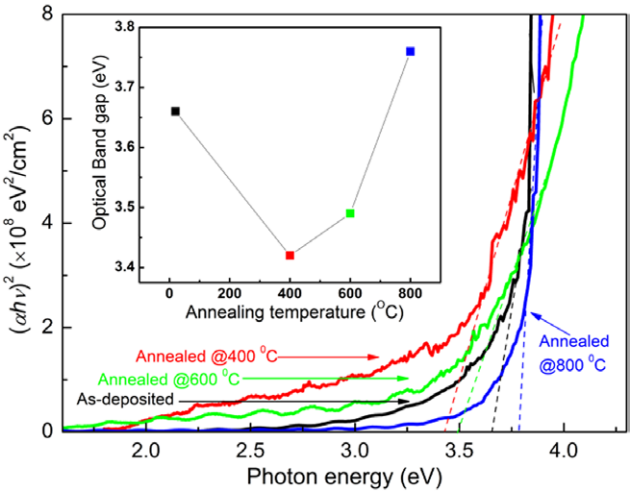

Figure 5. Optical absorption spectra of the as-deposited and annealed SnO_2 thin films. The inset shows the optical bandgap as a function of the annealing temperature.

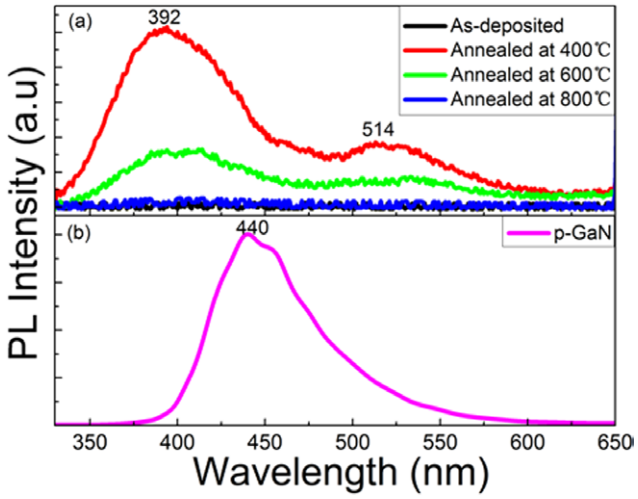

Figure 6. Room temperature PL spectra of (a) the as-deposited, 400, 600 and 800 °C annealed SnO_2 thin films and (b) the p-type GaN substrate.

Table 2. Electrical properties of the as-deposited and annealed SnO_2 films.

Electrical parameters	As-deposited	Annealed at 400 °C	Annealed at 600 °C	Annealed at 800 °C
Carrier density (cm^{-3})	1.2×10^{19}	8.6×10^{18}	4.7×10^{18}	1.0×10^{18}
Hall mobility ($cm^2 V^{-1}s^{-1}$)	13.1	10.5	4.3	3.6
Resistivity (Ω cm)	4.5×10^{-2}	6.8×10^{-2}	3.0×10^{-1}	2.4
Carrier type	*n*	*n*	*n*	*n*

evaporation of the elements in the SnO_2 film annealed at 400 °C leads to a decrease in grain size and hence the formation of lattice disordering or an amorphous area at grain boundaries. Thus, for the 400 °C annealed SnO_2 film, the nanocrystals are surrounded by the amorphous matrix, forming a nanocrystal/amorphous hybrid structure. As the annealing temperature increases, recrystallization plays a more important role compared to the evaporation of the elements, so the crystallinity of the films becomes better and the crystalline grain size becomes larger again. Furthermore, to determine whether the composition changes with the annealing temperature, we also examined the proportion of Sn and O elements using EDS analysis, as listed in table 1. It was found that the stoichiometric proportion of the Sn and O elements of all films is slightly bigger than 1:2, suggesting that the composition is not associated with the annealed temperature.

The optical bandgap E_g can be deduced from optical absorption spectra measurements made with the Tauc plot method: $(\alpha h\nu) = A(h\nu - E_g)^n$, where $h\nu$ is the photon energy, A is a constant which does not depend on the $h\nu$ and n is the power coefficient taken as 1/2. The E_g is estimated by extrapolating the linear portion of $(\alpha h\nu)^2$ versus $h\nu$ plots to the $h\nu$-axis. The curve diagrams in regard to the $(\alpha h\nu)^2$ versus the $h\nu$ of all the films are shown in figure 5. The E_g values of the SnO_2 films are 3.66, 3.42, 3.49 and 3.76 eV. The inset in figure 5 shows the bandgap as a function of the annealing temperature. For the fully crystallized SnO_2 films, the optical bandgaps are in agreement with the reported values of the bulk SnO_2 (3.6–3.8 eV). For the nanocrystal/amorphous SnO_2 film, the optical bandgap is 3.42 eV, smaller than the optical bandgap of the bulk SnO_2 and closer to the fundamental bandgap (the energy difference between the conduction-band minimum and the valence-band maximum), indicating that the dipole-forbidden rule is broken.

The room temperature PL emission spectra of the as-deposited and annealed SnO_2 films are shown in figure 6(a). For the as-deposited SnO_2 film, no emission peak is observed between 330 nm and 650 nm, which is caused by the dipole-forbidden rule of bulk SnO_2. After being annealed at 400 °C, the SnO_2 film could emit UV light. The two emission peaks are located at 392 and 514 nm, respectively. The UV emission peak is stronger than the visible emission one. The visible emission band is ascribed to the radiative recombination relevant to the deep level defects, such as the oxygen vacancy (Vo) [10, 37]. The SnO_2 film becomes a nanocrystalline/amorphous hybrid structure after being annealed at 400 °C, during which numerous dangling bonds existing at the surface of the nanoparticles with a high surface-to-volume ratio are buried in the surrounding amorphous matrix. The dangling bonds give rise to shallow states for ionic oxides [38], and the associated bound excitons are responsible for the UV emission.

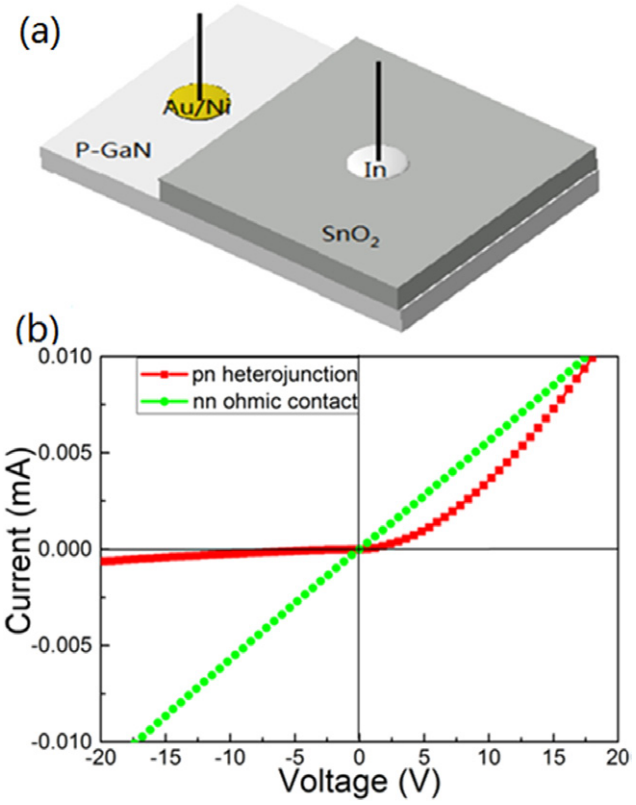

Figure 7. (a) Schematic diagram of the SnO_2/p-GaN heterojunction LED. (b) Room temperature *I–V* curves of the SnO_2/p-GaN heterojunction and *n–n* ohmic contact in the SnO2/p-GaN LED.

The observed UV emission indicates that the dipole-forbidden rule is broken by making the SnO_2 film become a nanocrystalline/amorphous hybrid structure. With the increase in the annealing temperature, the grains become larger and the crystallinity becomes better. The buried dangling bond defect states become fewer, and because the band structure of the nanostructured ionic semiconductors is sensitive to how the surfaces are passivated, the emission light intensity weakens and even disappears, for the 600 and 800 °C annealed films.

The observed variation in the electrical parameters of SnO_2 films annealed at different temperatures is given in table 2. All the SnO_2 films are n-type semiconductors. It is noted that the charge carrier density and mobility decrease with the increases in the annealing temperature. Carrier density is found to decrease with an increase in the annealing temperature due to the compensation of the oxygen vacancy. The mobility is affected by several scattering mechanisms involving neutral impurities, ionized impurities, grain boundaries and lattice vibration scattering. The decrease in carrier mobility is impacted by the increase in the grain boundary scattering due

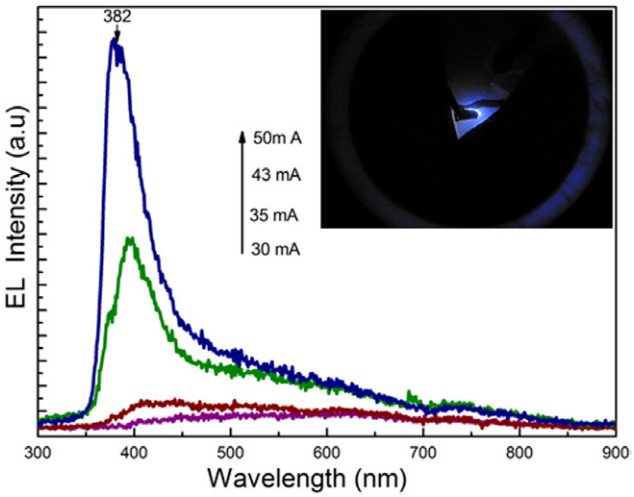

Figure 8. Room temperature EL spectra of the SnO_2/p-GaN heterojunction LED under various forward excitation currents. The inset shows a photograph of the LED biased forward current of 50 mA.

to the decreased grain size with the annealing temperature; therefore the electrical resistivity increases.

In order to apply SnO_2 nanomaterial to UV LEDs, the SnO_2 film was deposited on a p-GaN substrate and then annealed at 400 °C to form a SnO_2/p-GaN heterojunction with a SnO_2 nanocrystal/amorphous hybrid structure. The schematic diagram of the SnO_2/p-GaN LED prototype is shown in figure 7(a). Figure 7(b) shows the current–voltage characteristics of the SnO_2/p-GaN heterojunction, and good rectification is obtained in the heterojunction. The turn-on voltage is about 3.5 V for the SnO_2/p-GaN heterojunction. To confirm that the rectification is inherent, we measured the contact type between the In and SnO_2 by injecting a current through the In–SnO_2–In (two In electrodes were pasted on the SnO_2 layer), and obtained the *I–V* curve as represented by the green line in figure 7(b). The relation between the current and voltage is linear, confirming that the In contacts to the n-SnO_2 layer are ohmic contacts. The ideality factor n is one of the very important parameters, which impacts on the electrical characteristics of the diodes. The value can be calculated using the equation: $[dV/d(\ln I)] \propto (nkT/q)$. According to the *I–V* data, the obtained value of the ideality factor is 2.3.

Figure 8 shows the room temperature EL spectra of the SnO_2/p-GaN heterojunction LED under various forward excitation currents. The EL intensity heightens with the increasing excitation current. As the small injection current is applied, a dominant visible emission band is observed. When the injection current increases, the UV peak starts to enhance and visible emission is suppressed. As the injection current reaches 50 mA, there is a strong UV emission peak located at 382 nm with full width at half maximum of 80 nm, which is consistent with the result in the PL spectra. It should be noted that the PL peak of the p-GaN is centered at 440 nm, as shown in figure 6(b), indicating the 382 nm emission is not derived from the GaN layer. It is worth noting that the UV EL peak at the large injection current of 50 mA exhibits a slight blueshift with respect to the PL peak but a redshift at the small injection current of 35 mA. This is attributed to the higher efficient radiative recombination at the band-edge induced by the larger excited current [39]. In our previous reports, the UV emission peaks at 398 and 449 nm were observed from the SnO_2/MgO/p-GaN heterojunction and SnO_2:In/p-GaN heterojunction LEDs, respectively. This is the first time an emission peak centered at 382 nm in the SnO_2/p-GaN heterojunction has been observed. Therefore, our present fabrication method has the advantage of being MgO layer-free and doping-free with respect to the previous method.

4. Conclusion

In summary, SnO_2 films with a nanocrystal/amorphous hybrid structure were deposited on quartz substrates, in which the dipole-forbidden rule is broken and UV band-edge emission is observed in the PL spectra. Using a similar method, an emission peak located at 382 nm is observed in the EL spectra of a SnO_2/p-GaN heterojunction LED. The emergence of an UV emission in the SnO_2 hybrid films is the result of structural modification. The surface states play an important role in breaking the dipole-forbidden rule for the nanostructure-engineered SnO_2. Our results suggest that the fabrication method may make SnO_2 have a wider application range in the future.

Acknowledgments

This work is supported by: the National Natural Science Foundation of China under Grant Nos. 10874178, 11074093, 61205038 and 11274135; the Specialized Research Fund for the Doctoral Program of Higher Education under Grant No. 20130061130011; the PhD Programs Foundation of the Ministry of Education of China under Grant No. 20120061120011; the Natural Science Foundation of Jilin Province under grant No. 201115013, and the National Fund for Fostering Talents of Basic Science under grant No. J1103202. This work was also supported by the High Performance Computing Center of Jilin University, China.

References

[1] Walsh A *et al* 2008 Nature of the band gap of In_2O_3 revealed by first-principles calculations and x-ray spectroscopy *Phys. Rev. Lett.* **100** 167402
[2] Peng H Y, Li Y F, Lin W N, Wang Y Z, Gao X Y and Wu T 2012 Deterministic conversion between memory and threshold resistive switching via tuning the strong electron correlation *Sci. Rep.* **2** 442
[3] Look D C, Hemsky J W and Sizelove J R 1999 Residual native shallow donor in ZnO *Phys. Rev. Lett.* **82** 2552
[4] Li Y F, Deng R, Yao B, Xing G Z, Wang D D and Wu T 2010 Tuning ferromagnetism in $Mg_xZn_{1-x}O$ thin films by band gap and defect engineering *Appl. Phys. Lett.* **97** 102506
[5] Jain M, Chelikowsky J R and Louie S G 2011 Quasiparticle excitations and charge transition levels of oxygen vacancies in hafnia *Phys. Rev. Lett.* **107** 216803
[6] Zhou H, Deng R, Li Y-F, Yao B, Ding Z-H, Wang Q-X, Han Y, Wu T and Liu L 2014 Wavelength-tuned light emission

via modifying the band edge symmetry: doped SnO_2 as an example *J. Phys. Chem.* C **118** 6365
[7] Snaith H J and Ducati C 2010 SnO_2-based dye-sensitized hybrid solar cells exhibiting near unity absorbed photon-to-electron conversion efficiency *Nano Lett.* **10** 1259
[8] Qian J, Liu P, Xiao Y, Jiang Y, Cao Y, Ai X and Yang H 2009 TiO_2-coated multilayered SnO_2 hollow microspheres for dye-sensitized solar cells *Adv. Mater.* **21** 3663
[9] Li Y F, Yin W J, Deng R, Chen R, Chen J, Yan Q Y, Yao B, Sun H D, Wei S H and Wu T 2012 Realizing a SnO_2-based ultraviolet light-emitting diode via breaking the dipole-forbidden rule *NPG Asia Mater.* **4** e30
[10] Li Y, Deng R, Tian Y, Yao B and Wu T 2012 Role of donor-acceptor complexes and impurity band in stabilizing ferromagnetic order in Cu-doped SnO_2 thin films *Appl. Phys. Lett.* **100** 172402
[11] Kowal A, Li M, Shao M, Sasaki K, Vukmirovic M B, Zhang J, Marinkovic N S, Liu P, Frenkel A I and Adzic R R 2009 Ternary Pt/Rh/SnO_2 electrocatalysts for oxidizing ethanol to CO_2 *Nat. Mater.* **8** 325
[12] Batzill M and Diebold U 2005 The surface and materials science of tin oxide *Prog. Surf. Sci.* **79** 47
[13] Agekyan V T 1977 Spectroscopic properties of semiconductor crystals with direct forbidden energy gap *Phys. Status Solidi* **43** 11
[14] Won II Park G-C Y 2004 Electroluminescence in n-ZnO nanorod arrays vertically grown on p-GaN *Adv. Mater.* **16** 87
[15] Edmond J *et al* 2004 High efficiency GaN-based LEDs and lasers on SiC *J. Cryst. Growth* **272** 242
[16] Feng Q-J, Liang H-W, Mei Y-Y, Liu J-Y, Ling C C, Tao P-C, Pan D-Z and Yang Y-Q 2015 ZnO single microwire homojunction light emitting diode grown by electric field assisted chemical vapor deposition *J. Mater. Chem.* C **3** 4678
[17] Iwan S, Zhao J L, Tan S T, Bambang S, Hikam M, Fan H M and Sun X W 2015 Ion-dependent electroluminescence from trivalent rare-earth doped n-ZnO/p-Si heterostructured light-emitting diodes *Mater. Sci. Semicond. Process.* **30** 263
[18] Li Y, Yao B, Deng R, Li B, Zhang Z, Shan C, Zhao D and Shen D 2013 A comparative study on electroluminescence from ZnO-based double heterojunction light emitting diodes grown on different lattice mismatch substrates *J. Alloys Compd.* **575** 233
[19] Lu Y-J, Shan C-X, Jiang M-M, Li B-H, Liu K-W, Li R-G and Shen D-Z 2014 Enhanced emission from ZnO-based double heterostructure light-emitting devices using a distributed Bragg reflector *RSC Adv.* **4** 16578
[20] Nguyen N T, Ri S-G, Nagata T, Ishibashi K, Takahashi K, Tsunekawa Y, Suzuki S and Chikyow T 2014 Epitaxial growth of nonpolar ZnO and n-ZnO/i-ZnO/p-GaN heterostructure on Si(0 0 1) for ultraviolet light emitting diodes *Appl. Phys. Express* **7** 062102
[21] Shih Y T, Wu M K, Chen M J, Cheng Y C, Yang J R and Shiojiri M 2009 ZnO-based heterojunction light-emitting diodes on p-SiC(4H) grown by atomic layer deposition *Appl. Phys.* B **98** 767
[22] Wu C, Liu F, Liu B, Zhuang Z, Dai J, Tao T, Zhang G, Xie Z, Wang X and Zhang R 2015 Enhanced opto-electrical properties of graphene electrode InGaN/GaN LEDs with a NiO_x inter-layer *Solid-State Electron.* **109** 47
[23] Zhang Q, Guo H, Feng Z, Lin L, Zhou J and Lin Z 2010 n-ZnO nanorods/p-CuSCN heterojunction light-emitting diodes fabricated by electrochemical method *Electrochim. Acta* **55** 4889
[24] Chen R, Xing G Z, Gao J, Zhang Z, Wu T and Sun H D 2009 Characteristics of ultraviolet photoluminescence from high quality tin oxide nanowires *Appl. Phys. Lett.* **95** 061908
[25] He J H, Wu T H, Hsin C L, Li K M, Chen L J, Chueh Y L, Chou L J and Wang Z L 2006 Beaklike SnO_2 nanorods with strong photoluminescent and field-emission properties *Small* **2** 116
[26] Kar A, Stroscio M A, Dutta M, Kumari J and Meyyappan M 2009 Observation of ultraviolet emission and effect of surface states on the luminescence from tin oxide nanowires *Appl. Phys. Lett.* **94** 101905
[27] Liu B, Cheng C W, Chen R, Shen Z X, Fan H J and Sun H D 2010 Fine structure of ultraviolet photoluminescence of tin oxide nanowires *J. Phys. Chem.* C **114** 3407
[28] Yang H Y, Yu S F, Lau S P, Tsang S H, Xing G Z and Wu T 2009 Ultraviolet coherent random lasing in randomly assembled SnO_2 nanowires *Appl. Phys. Lett.* **94** 241121
[29] Yang H Y, Yu S F, Tsang S H, Chen T P, Gao J and Wu T 2009 High temperature excitonic lasing characteristics of randomly assembled SnO_2 nanowires *Appl. Phys. Lett.* **95** 131106
[30] Deng R, Li Y-F, Yao B, Ding Z-H, Fang X, Qin J-M, Wei Z-P, Liang Q-C and Liu L 2015 Recovering near-band-edge ultraviolet responses in a wide-bandgap oxide with dipole-forbidden bandgap transition *J. Alloys Compd.* **649** 625
[31] Khan A F, Mehmood M, Aslam M and Ashraf M 2010 Characteristics of electron beam evaporated nanocrystalline SnO_2 thin films annealed in air *Appl. Surf. Sci.* **256** 2252
[32] Ningthoujam R S and Kulshreshtha S K 2009 Nanocrystalline SnO_2 from thermal decomposition of tin citrate crystal: Luminescence and Raman studies *Mater. Res. Bull.* **44** 57
[33] Yang C C and Li S 2008 Size-dependent Raman red shifts of semiconductor nanocrystals *J. Phys. Chem.* B **112** 14193
[34] Hosono H,Mizuguchi M and Skuja L andOgawa T1999 Fluorine-doped SiO_2 glasses for F2 excimer laser optics: fluorine content and color-center formation *Opt. Lett.* **24** 1549
[35] Hemmati M, Chizmeshya A, Wolf G H, Poole P H, Shao J and Angell C A 1995 Crystalline-amorphous transition in silicate perovskites *Phys. Rev.* B **51** 14841
[36] Fujii Y, Kowaka M and Onodera A 1985 The pressure-induced metallic amorphous state of SnI_4. I. A novel crystal-to-amorphous transition studied by x-ray scattering *J. Phys. C: Solid State Phys.* **18** 789
[37] Kılıç Ç and Zunger A 2002 Origins of coexistence of conductivity and transparency in SnO_2 *Phys. Rev. Lett.* **88** 095501
[38] Walsh A, Da Silva J L F and Wei S-H 2009 Interplay between order and disorder in the high performance of amorphous transparent conducting oxides *Chem. Mater.* **21** 5119
[39] Li L, Li P, Wen Y, Wen J and Zhu Y 2009 Temperature dependences of photoluminescence and electroluminescence spectra in light-emitting diodes *Appl. Phys. Lett.* **94** 261103